Desalination and Water Treatment
www.deswater.com

doi:10.5004/dwt.2017.21063

83 (2017) 133–143
July

Optimization of lead ions adsorption on hydrolyzed polyacrylonitrile fibers using central composite design

Parvin Karimineghlani[a,*], Paria Karimi Neghlani[b], Amirreza Azadmehr[c]

[a]*Department of Material Science and Engineering, Texas A&M University, College Station, TX 77843, USA, email: karimi@tamu.edu*
[b]*Department of Engineering Science, University West in Sweden, Trollhattan, Sweden, 46153, email: paria.karimi-neghlani@hv.se*
[c]*Department of Mining and Metallurgical Engineering, Amirkabir University of Technology, Tehran, Iran, 15875-4413, email: a_azadmehr@aut.ac.ir*

Received 2 October 2016; Accepted 24 June 2017

ABSTRACT

Optimization of lead ions (Pb^{++}) adsorption on the hydrolyzed polyacrylonitrile (PAN) fibers was reported by using statistical approach. Electrospinning of PAN solutions in dimethylformamide (DMF) was performed with different concentrations. The electrospun fibres, with various diameters, were then hydrolyzed in a sodium hydroxide solution (NaOH) for different reaction times and temperatures. Response surface methodology (RSM) helped optimizing the hydrolysis reaction conditions to maximize the adsorption capacity of the PAN fibers. The maximum value of adsorption capacity was experimentally determined to be 141 mg/g with the optimized values of hydrolysis reaction time, temperature and fiber diameter being 61.6°C, 82.1 min and 280 nm, respectively. The as-prepared electrospun fibers, hydrolyzed fibers and fibers after adsorption process were characterized by scanning electron microscope (SEM). Experimental adsorption data fit very well with the Langmuir isotherm model. It was found that Pb^{++} ions adsorption on the nanofibers was 20 times higher than that on microfibers under the same conditions. Adsorption kinetics followed the second order kinetics model.

Keywords: Nanofibers; Hydrolysis; Polyacrylonitrile; Central composite design; Adsorption; Lead ion

1. Introduction

Heavy metals are considered one of the important pollutants of the environment causing water contamination. Therefore, they are a real threat to human health. Typically, adsorption is regarded as a common method to remove toxic metal ions. Removal of metal ions from aqueous solutions is usually controlled by surface functional groups of the adsorbents [1].

Activated carbon, oxide minerals, polymeric fibers, resins, and biosorbents have been applied as the common adsorbents to remove metal ions or recover precious metals [2–11]. Recently, modified polymeric fibers have been used extensively to remove heavy metals from water and wastewater. Modified fibers that contain tetrazine, carboxyl, imidazoline, amidoximeoramino were shown to be effective in this area [2,3,5].

*Corresponding author.

In 1934 electrical forces were first applied to make polymeric fibers [12]. Later on, this method was called electrospinning. A typical electrospinning setup includes a high voltage power supply, an injector (syringe), and a grounded metal collector. After applying high voltage to a polymer solution, deformation of a drop of solution (conic form called Taylor cone) at the syringe tip starts to happen. Over a critical voltage, the electrical force at the surface of the drop overcomes solution surface tension and intermolecular interactions. As a result, the polymer solution is extended and elongated into fibers, which are deposited as a non-woven maton the collector [6,13–17]. It is possible to produce fibers with diameters less than 400 nm, called nanofibers. Nanofibers have appealing properties, such as a high porosity, high gas permeability and, most importantly, a large specific surface area, in comparison to the traditional fibers. Hence, electrospinning has been given noticeable attention over the past decades. Nanofibers mostly have been studied for applications such as nanocomposites [18,19], tissue engineering [20,21], sensors [22],

and adsorptive membranes [23,24]. Possessing large specific surface area is one of the important features of the adsorptive nanofibers [24–27].

Recently, many researchers have studied the metal ion adsorption behavior of functionalized PAN nanofibers [28–32]. Bode-Aluko et al. [30] reviewed past research about the adoption process of toxic metal ions on the modified PAN nanofibers. They have reported many studies, which sought to reach a high value of metal ion adsorption using PAN nanofibers. Based on their findings, the adsorption efficiency is influenced by various parameters such as dimension of fibers, type and percentage of functional groups, adsorption reaction temperature, pH and adsorption time. However, to the best of our knowledge, our work is the first study based on design of experiment (DoE) on the Pb^{++} ions adsorption by hydrolyzed polyacrylonitrile (HPAN) nanofibers to find the optimum amount of metal ion adsorption with no loss of physical properties of fibers. In the present work, optimization of Pb^{++} ions adsorption on the HPAN microfibers and nanofibers was conducted using a statistical approach in order to determine the experimental parameters for maximum adsorption of Pb^{++} ions. A three factors with three levels central composite design (CCD) method was chosen, due to its simplicity. Those three key factors were hydrolysis reaction temperature, reaction time and fibers diameter. The optimum condition was determined in order to have the maximum adoption on PAN fibers with no sample quality loss. Atomic absorption spectroscopy (AAS) was applied to measure Pb^{++} ions concentration in the solution. Scanning electron microscopy (SEM) was used to show the nanofiber surface morphology changes before and after processing. A pseudo-second order kinetics model is presented for the adsorption kinetics. Pb^{++} ions adsorption on the nanofibers was compared to that on microfibers under the same conditions. Moreover, the Pb^{++} ions adsorption mechanism was studied.

2. Materials and methods

2.1. Materials

PAN microfibers, a copolymer of 93.7% acrylonitrile and 6.3% methylacrylate with M_v = 70000 g/mol, were purchased from Isfahan Polyacryl Inc, Iran. Dimethyl formamide (DMF), as PAN solvent, sodium hydroxide, (NaOH), as hydrolysis agent, and ethanol were all supplied by Merck Co., Germany. Lead nitrate, ($Pb(NO_3)_2$), also supplied by Merck Co., was used to prepare lead ion aqueous solutions for adsorption studies.

2.2. Instruments

An attenuated total reflection Fourier transform infrared (ATR-FTIR) spectrometer, EQUINOX 55, from Bruker (Germany), was used for chemical characterization in the wavenumber range of 400–4000 cm^{-1}. A model 939 Unicam atomic absorption spectrophotometer was used to determine lead ion concentration. The surface morphologies of the platinum/palladium alloy-coated PAN and HPAN nanofibers were studied using Tescan FERA-3 SEM. pH levels were measured with a pH-meter (Hach Instrument).

2.3. Design of experiments

Design of experiment has mostly been employed in various fields such as chemistry, agriculture, biology, economy, etc. Response Surface Methodology (RSM), a well-known method for design of experiment, is a sequential statistical method that allows for a minimum number of experiments and cost to extract meaningful information [33–36]. Previously, the adsorption process was studied based on the full factorial approach [6,37]. However, RSM reduces the required number of experiments and optimizes the process. CCD, the most used design method in RSM, can develop an appropriate empirical relationship [38]. It requires the use of a two-level factorial design with 2^k points combined with 2k axial points and n center runs, k being the number of factors. The total number of experiments, N, with k factors is:

$$N = 2^k + 2k + n. \quad (1)$$

The CCD was used in combination with a second-order model. The second-order model is widely used because it is easy to estimate model parameters and there have been many practical applications in solving the real response surface problems [35,39]. In this research the hydrolysis reaction temperature, time and fibers diameter were the three selected factors.

Three levels were selected for each factor, see Table 1. The levels of the factors were coded as −1 (low), 0 (central point) and 1 (high). According to the CCD, 17 experiments were performed as shown in Table 2. Using statistical analysis,it is possible to sort the factors and their interactions based on their relative importance to the response. The general form of the second order model is as follows:

$$y = b_0 + b_1x_1 + b_2x_2 + b_3x_3 + b_{11}x^2_1 + b_{22}x^2_2 + b_{33}x^2_3 + b_{12}x_1x_2 + b_{13}x_1x_3 + b_{23}x_2x_3 \quad (2)$$

where y is the predicted response and x_1, x_2, x_3 are the three factors. b_i and b_{ij} are regression coefficients. All associated calculations were carried out using the Design Expert software (Version 10, State-Ease Inc., USA).

2.4. Electrospinning of PAN nanofibers

PAN nanofibers were produced by electrospinning method. 10 and 12 wt% solutions of PAN in DMF were prepared by stirring at room temperature for 24 h. The electrospinning was performed under ambient conditions using a fixed collector, applied voltage of 20 kV and a feeding rate of 200 μL/h. The distance between the syringe tip and the collector was 15 cm. At the end, PAN nanofibers were col-

Table 1
The coded values of the three independent factors

	Levels		
	–1	0	1
Reaction temperature (°C)	55	65	75
Contact time (min)	60	90	120
Average fiber diameter (nm)	110	1000	1900

lected on the collector in the form of a non-woven mat. In this study, electrospinning conditions were selected based on previous publications [15,16].

2.5. Hydrolysis reaction

1 g of fibers was immersed in a mixture of 300 ml of ethanol/water solution having 10% (w/w) NaOH in a beaker. Reactions were performed according to the experiment conditions listed in Table 2. Afterwards, the fibers were rinsed with distilled water until a pH level of 7 was reached and then were dried at 70°C in an oven.

2.6. Adsorption experiments

Adsorption measurements were conducted batch-wise. Metal ion adsorption amount and the time that adsorption reached to equilibrium (t_e) were determined using AAS. HPAN fibers (with equal total areas) were added to the lead nitrate aqueous solution with the initial concentration of 590 ppm. The solution was mixed at 60 rpm and 25°C. Sample concentrations were measured at 10, 20, 30, 60, 120 and 180 min. At t_e, the adsorbed lead ions (mg/g) was quantified based on the following equation, [13]:

$$q = \frac{(C_0 - C_f)V}{M} \quad (3)$$

where q is the adsorbed lead ions, (mg/g), V is the solution volume (l), M is the amount of added adsorbent (g), and C_0, and C_f are the initial and final lead ion concentrations (mg/l), respectively. For evaluation of the effect of pH levels on the metal ion adsorption, the initial lead ion concentration in the solutions was kept at 590 ppm.

3. Result and discussion

3.1. Hydrolysis reaction mechanism

ATR-FTIR spectroscopy was used to study the changes in the PAN structure during hydrolysis. IR spectra of PAN and HPAN fibers are shown in Fig. 1. The PAN spectrum

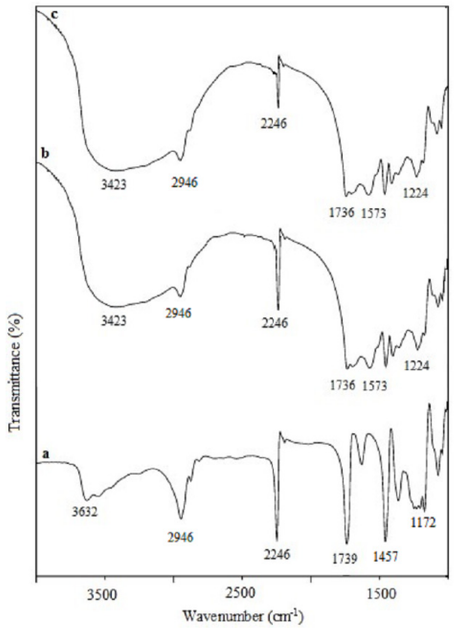

Fig. 1. ATR-FTIR spectra of fibers with different average diameters: (a) PAN, (b) HPAN with 1 μm and (c) HPAN with 110 nm.

Table 2
Reaction conditions, adsorption amount and appearance properties of hydrolyzed PAN fibers mats (C_0=590 ppm)

Experiment No	Temperature (x_1)	Time (x_2)	Fiber diameter (x_3)	Actual adsorption (mg/g)	Predicted adsorption (mg/g)	Appearance Properties
1	–1	–1	–1	35.82	24	Soft-light yellow
2	1	–1	–1	85.12	84	Soft-Dark orange
3	–1	1	–1	134.1	123	Rigid-Dark orange
4	1	1	–1	Damaged	183	Brittle-white
5	–1	–1	1	1.69	0	Soft-light yellow
6	1	–1	1	7.03	2.52	Soft-Dark orange
7	–1	1	1	4.62	2.76	Rigid-Dark orange
8	1	1	1	22.78	13.8	Soft-Dark orange
9	–1	0	0	102.12	87	Rigid-Dark orange
10	1	0	0	141	123	Rigid-Dark orange
11	0	–1	0	69.28	69	Rigid-Dark orange
12	0	1	0	135.41	123	Rigid-Dark orange
13	0	0	–1	130.11	114	Soft-light yellow
14	0	0	1	5.97	0.12	Soft-light yellow
15	0	0	0	112.26	105	Soft-light yellow
16	0	0	0	111.1	105	Soft-light yellow
17	0	0	0	112	105	Soft-light yellow

(curve a) has peaks corresponding to stretching vibrations at 2246 cm^{-1} (C–N), 1739 cm^{-1} (C=O), 1172 cm^{-1} (C–N) and 2946 cm^{-1} (C–H). 1457 cm^{-1} peak corresponds to the –CH bending. These observations confirm that PAN is a copolymer of acrylonitrile and methylacrylate.

The intensity of the nitrile group peak at 2246 cm^{-1} decreased with the hydrolysis reaction progress (shown in Figs. 1b, 1c). The peak at 3632 cm^{-1}, which is assigned to the stretching vibration of –OH groups [40], was shifted to 3423 cm^{-1} and the intensity of the peak increased extensively. This change shows the introduction of –OH groups on the PAN molecules. At the same time, two new peaks at 1573 and 1224 cm^{-1} appeared, corresponding to the imine conjugated groups in the hydrolyzed fibers. This result is consistent with the previous studies [5]. Therefore, it is suggested that the nitrile groups of PAN were first hydrolyzed into imine groups (–C=NH, Fig. 2) and then went through a cyclization reaction. Moreover, the C=O peak of ester groups at 1739 cm^{-1} and $–CH_2$ stretching peak at 2946 cm^{-1} were reduced that show acetate ester groups were removed from the surface of PAN fibers [5].

The IR analysis confirmed that the hydrolysis of PAN nanofibers was achieved almost completely (Fig. 1c). However, as shown in Fig. 1b PAN microfibers were reacted only partially. The proposed corresponding chemical mechanism during hydrolysis is shown in Fig. 2. The nitrile group peak (2246 cm^{-1}) nearly disappeared for the HPAN nanofibers, as shown in Fig.1c. Hence, conversion was almost complete.

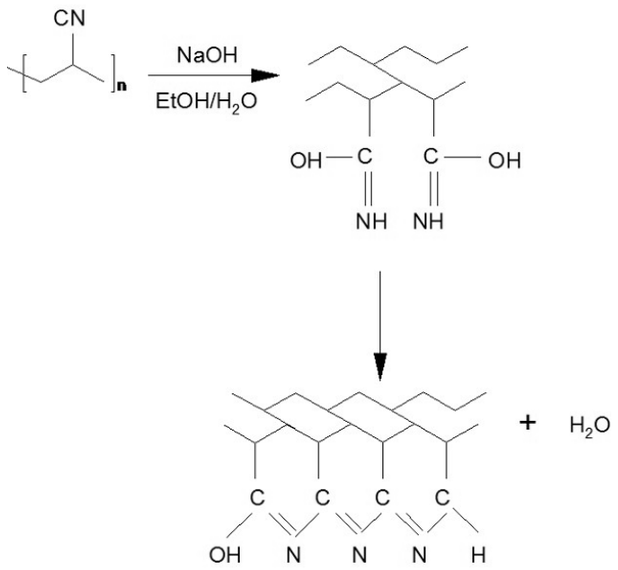

Fig. 2. Hydrolysis reaction mechanism of PAN fibers.

3.2. Response surface method

RSM allows development of a mathematical model in order to relate adsorption amount (y), as response variable, to the hydrolysis reaction temperature (x_1), hydrolysis reaction time (x_2) and average fiber diameter (x_3) [41]. The CCD results for the three factors with three various levels selected in this study are shown in Table 2. Table 3 gives the preliminary results of ANOVA.

The b_{11} and b_{12} coefficients were non-significant and eliminated from the model. The revised statistical parameters

Table 4
Revised statistical parameters obtained from the ANOVA

Source	Sum of squares	D_f	Mean square	F-value	P-value
Model	0.57	7	0.081	149.52	< 0.0001
x_1	0.035	1	0.035	64.58	< 0.0001
x_2	0.086	1	0.086	158.34	< 0.0001
x_3	0.29	1	0.29	526.27	< 0.0001
x_1x_3	0.013	1	0.013	24.78	0.0008
x_2x_3	0.044	1	0.044	80.99	< 0.0001
x_2^2	0.002882	1	0.002882	5.31	0.0467
x_3^2	0.06	1	0.06	110.71	< 0.0001
Residual	0.004884	9	0.000542		
Lack of fit	0.004768	7	0.000681	11.68	0.0811
Pure error	0.0001167	2	0.000058		
Total	0.57	16			

Table 3
Statistical parameters obtained from the ANOVA

Source	Sum of squares	D_f	Mean square	F-value	P-value	
Model	0.57	9	0.063	130.06	< 0.001	Significant
x_1	0.035	1	0.035	72.04	< 0.0001	Significant
x_2	0.086	1	0.086	176.63	< 0.0001	Significant
x_3	0.29	1	0.29	587.07	< 0.0001	Significant
x_1^2	0.001269	1	0.001269	2.61	0.1504	Not Significant
x_2^2	0.003918	1	0.003918	8.05	0.0251	Significant
x_3^2	0.059	1	0.059	121.02	< 0.0001	Significant
x_1x_2	0.0002101	1	0.0002101	0.43	0.5321	Not Significant
x_1x_3	0.013	1	0.013	27.64	0.0012	Significant
x_2x_3	0.044	1	0.044	90.35	< 0.0001	Significant

obtained from the ANOVA are shown in Table 4. The results were analyzed using ANOVA to assess the goodness of fit with the results given in Table 4. F-tests were performed and terms at the 5% significance level (Prob < 0.05) were included in the model. In other words, only statistically significant terms were kept in the model.

The reduced form of the quadratic regression model, in coded values, was as the following equation:

$$\hat{y}_Q = 0.35 + 0.059x_1 + 0.093x_2 - 0.17x_3 - 0.031x_2^2 - 0.14x_3^2 - 0.041x_1x_3 - 0.074x_2x_3 \quad (4)$$

Model correlation coefficient, R^2, and adjusted R^2 were 0.9915 and 0.9848, respectively; R^2 and adjusted R^2 were in very good agreement. Therefore, the model is a very good representation of the experimental data. The ratio of the standard error of estimation to the mean value of the observed response is defined as the coefficient of variance (CV, expressed in percentage). CV value less than 10% indicates reproducibility of the model [42]. In this study, the CV was found to be 9.37%. The adequate precision value as a measure of the "signal-to-noise ratio" was found to be 40.16, which shows an adequate signal. A ratio greater than 4 is desirable [43].

The relative contribution of each term (i.e. temperature, time and fiber diameter) of the model is directly measured by the coefficient of that term. The positive sign for the coefficients of reaction temperature (x_1) and time (x_2) indicated that metal ion adsorption increases with increase of x_1 from 55 to 75°C and x_2 from 60 to 120 min [shown in Eq. (4)]. However, the model shows that the lead ion adsorption decreases with an increase in fiber diameter (x_3), keeping the other terms constant.

The model also provided the predicted values for lead ions adsorption by the hydrolyzed fibers, which are included in Table 2. Experimentally measured data for adsorption are also given in Table 2. Three-dimensional and contour plots of the model give a graphical representation of interactions between variables [36,44]. The response is plotted versus fiber diameter and reaction time in Fig. 3. In addition, in Fig. 4 response is plotted vs. reaction tempera-

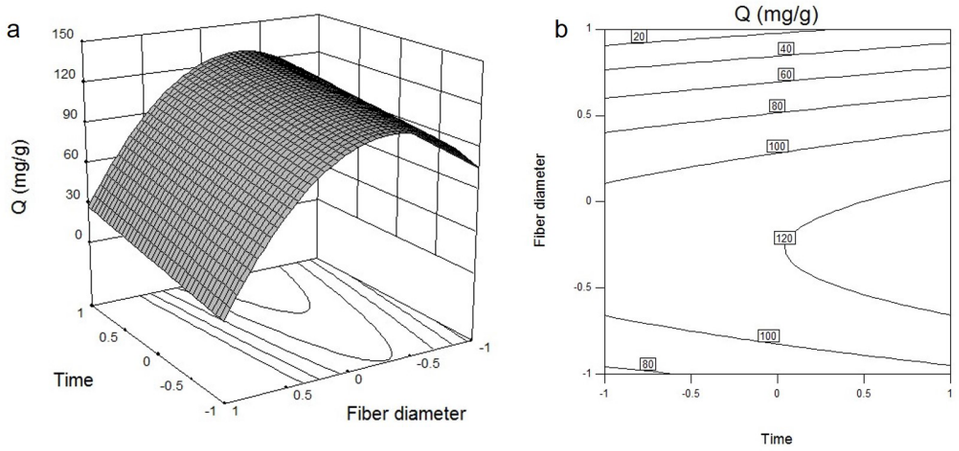

Fig. 3. Scheme of (a) Response surface and (b) contour plot of adsorption amount versus time and fiber diameter, reaction temperature held at 65°C.

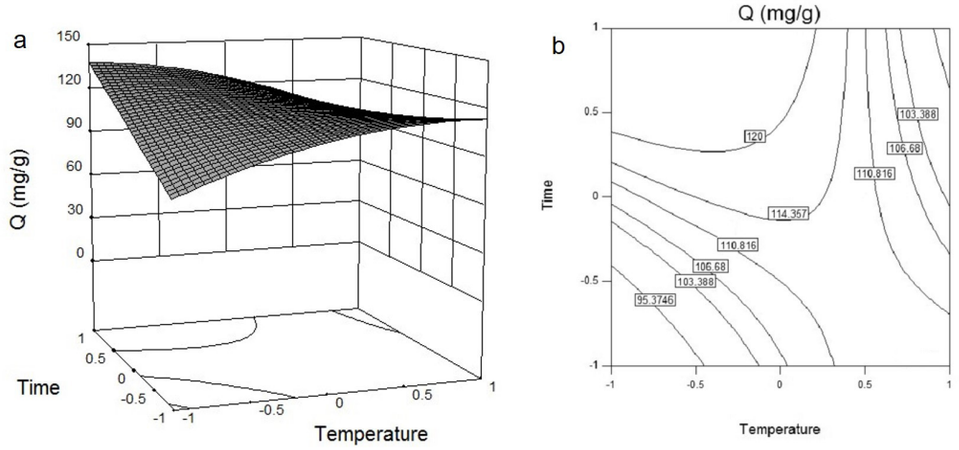

Fig. 4. Scheme of (a) Response surface and (b) contour plot of adsorption amount versus time and temperature, fiber diameter kept at 1 µm.

ture and time. The adsorption amount increased almost linearly as the reaction time and temperature increased to a high level, while a curvature type relationship existed between adsorption amount and fiber diameter (Fig. 3). The adsorption amount decreased as the fiber diameter increased toward a high level, i.e.1.9 μm. The contour plots confirmed these results (Figs. 3b and 4b).

Previous works on PAN fibers reported similar trends; as the time and temperature of functionalization reaction was increased, the adsorption amount of a given fiber sample increased linearly [37]; however, at smaller diameters, fibers have a higher specific surface area and as a consequence, more functionalization and adsorption can take place [32]. In the model for adsorption amount of lead ions on HPAN fibers, fiber diameter (x_3) was the major factor affecting the response (largest coefficient magnitude, $b_3 = -0.17$).

3.3. Optimization of hydrolysis conditions

Table 2 shows the results of Pb^{++} ions adsorption for the conducted experiments along with the appearance of the hydrolyzed fibers. Depending on the hydrolysis conditions, the color of the fibers was shown to change from white to light yellow and then dark orange. The white color of the fibers at high temperatures and longer times could be attributed to the degradation of nitrile groups. With increasing degree of hydrolysis, the fiber mats become fragile and less capable of adsorbing Pb^{++} ions (Fig. 5). In fact, after hydrolysis, there is a decrease in polymer chains flexibility and mobility. Hence, crystallization and mechanical properties are deteriorated [33]. This observation is consistent with the previously reported results [6,32,45].

Hydrolysis of nitrile groups in PAN was increased by increasing time and temperature of the reaction. Raising the temperature accelerates the hydrolysis reaction of PAN fibers significantly and can be due to the endothermic nature of the adsorption reaction that was reported in other studies [6,32]. The efficiency of the hydrolysis process depends on the specific surface area of the fibers, too. Nanofibers have larger specific surface area than microfibers. Referring to IR results shown in Figs. 1b and 1c, upon decreasing fiber diameter, the nitrile groups' hydrolysis increased.

The second-degree polynomial equation, Eq. (4), was solved using the numerical optimization feature of Design Expert 10 software to find the optimum conditions for adsorption of lead ions. In order to set the criteria for optimization of all variables, the software uses five possibilities for a "goal" to construct a desirability index. The numerical optimization function of the Design Expert combines the individual desirability into a single number and then looks for the highest overall desirability (desirability ranges from zero to one for the response). A "target" possibility was used in the present study. The target goal was set to 141 mg/g. The optimum values of the test variables for this adsorption amount (141 mg/g) were obtained, in coded values, as $x_1 = -0.34$, $x_2 = 0.57$, $x_3 = -0.80$ and these values were converted to un-coded values i.e., actual values, $x_1 = 61.6$°C, $x_2 = 82.1$ min, $x_3 = 280$ nm. These results show that, by reducing the fiber diameter, we could reach the same adsorption amount in lower time and at lower temperature.

Running the adsorption experiments under the optimum conditions calculated for the three parameters, 132 mg/g of Pb^{++} ions adsorption was obtained for PAN nanofibers. This experimental value closely agrees with the values obtained from the RSM method. These results confirm that the statistical design of experiments by using RSM could be effectively used to optimize the process parameters and to study the importance of individual, cumulative and interactive effects of the test variables on the hydrolysis process.

Highly hydrolyzed PAN nanofibers form fragile sheets, which were not applicable for metal ion adsorption (Fig. 5). Thus, samples with 141 mg/g adsorption amount had the highest metal uptake. This value is 4.5 times the reported value, 30 mg/g, for PAN microfibers hydrolyzed with NaOH [5]. Based on our experiments results, at the same conditions, nanofibers can adsorb 20 times more Pb^{++} ions than microfibers, as shown in rows 13 and 14 in Table 2.

3.4. pH and time effects on the adsorption

3.4.1 Effect of pH

It is well known that pH level has a major impact on the metal ions adsorption process [31,46–48]. Effect of pH value on the Pb^{++} ions adsorption is shown in Fig. 6. For pH levels less than 2, there was no noticeable adsorption of lead ions. The adsorption amount of lead ions on the HPAN nanofiber increased with the increase of the pH from 2 to 5. Maximum adsorption of Pb^{++} ions happened in the pH levels between 4 and 5. At low pH, the high H^+ concentration competes with the metal ion in being adsorbed. In addition, the adsorbed hydrogen ions repel the metal ions. On the other hand, Pb^{++} ions adsorption started to decrease beyond pH 5. This decrease could be due to the hydrolysis of Pb^{++} ions in the form of $Pb_2(OH)_2^{2+}$, $Pb(OH)^+$ and $Pb(OH)_2$ in the basic solutions [5,7].

3.4.2. Effect of contact time

Fig. 7 shows the results of adsorption of lead ions onto the HPAN nanofibers and microfibers as a function of time (up to 2 h). Our results showed that the adsorption process on the nanofibers was about 3 times faster than that in microfibers.

The equilibrium values of lead ions adsorption on the modified nanofibers and microfibers were about 102.12 and 22.78 mg/g, respectively. Therefore, in this condition, nanofibers showed over 5 times more metal ion adsorption in comparison with microfibers. It is worth mentioning that the microfibers were hydrolyzed even for a longer time and

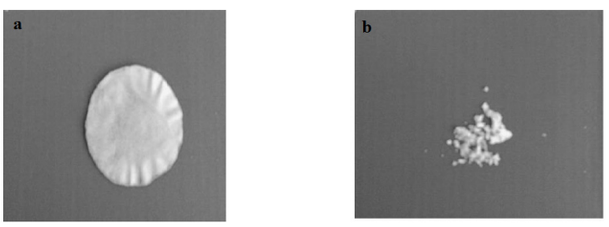

Fig. 5. Hydrolyzed nanofibers at (a) 55°C and 60 min (b) 75°C and 120 min.

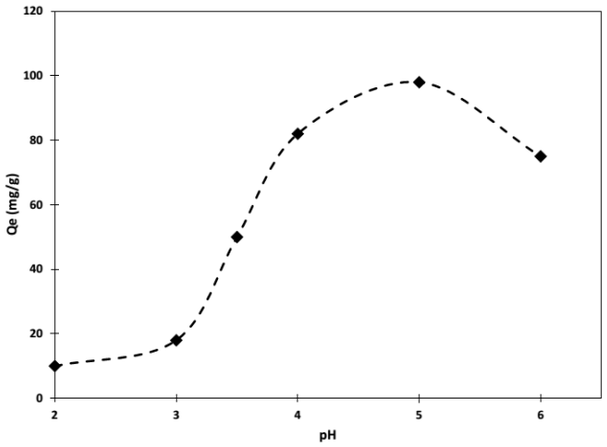

Fig. 6. Effect of solution pH on the adsorption of Pb^{++} ions on the HPAN nanofibers (t = 1 h, C_0 = 590 ppm).

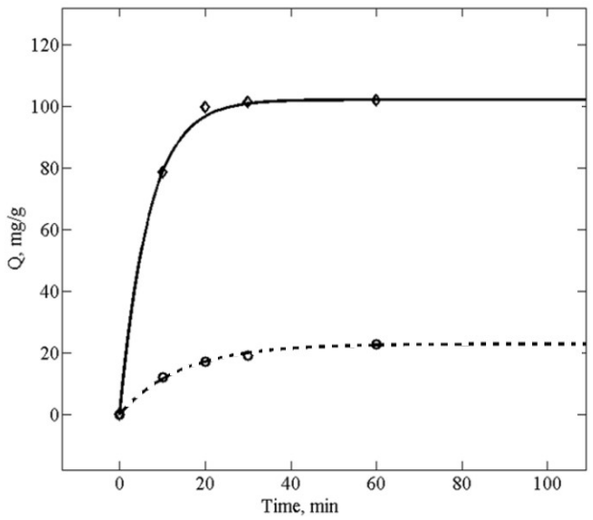

Fig. 7. Adsorption of lead ions (vs. time) on (o) HPAN microfiber (hydrolyzed at T = 65°C, t = 90 min), (◊) HPAN nanofiber (hydrolyzed at T = 55°C, t = 60 min), C_0 = 590 ppm.

at a higher temperature. This observation could be related to more adsorption sites on the HPAN nanofibers [7].

3.5. Morphology studies

The morphology of as-spun PAN nanofibers, HPAN nanofibers before and after the metal ion adsorption was characterized using the SEM technique. The samples were sputter coated with a thin layer of platinum/palladium alloy nanoparticles to reduce the charging effects. PAN nanofibers showed a smooth surface with no bead formation (Fig. 8a). After hydrolysis, the fibers still show smooth surface with no crack or physical damage. However, the overall structure shows that fibers are attached together at some points, which could be the effect of chemical reaction (Fig. 8b). One interesting point was that some impurities appeared on the HPAN nanofibers after metal ion adsorption. One possible hypothesis is that these impurities are formed as a complex between lead ions and platinum/palladium alloy nanoparticles. The possible interactions of lead ions with platinum and palladium have been reported previously [49–51]. Observation of clustered impurities (~200 nm) which occurred after coating and only observed with samples after metal ions adsorption can be strong evidence of Pb^{++} ions adsorption.

3.6. Adsorption isotherms

An adsorption isotherm at equilibrium can be evaluated as the relation of the adsorbate concentration on the fiber surface and in the solution at a constant temperature. Isotherm data should accurately fit into those isotherm models which are appropriate models for further process studies [52]. The Langmuir and Freundlich isotherms are two models that frequently have been applied in this area. These equations are as follows, respectively:

$$Q_e = \frac{Q_m b C_e}{1 + b C_e} \tag{5}$$

$$Q_e = K C_e^{1/n} \tag{6}$$

where C_e is the equilibrium concentration (mmol/L), b is the Langmuir constant which is related to the binding energy

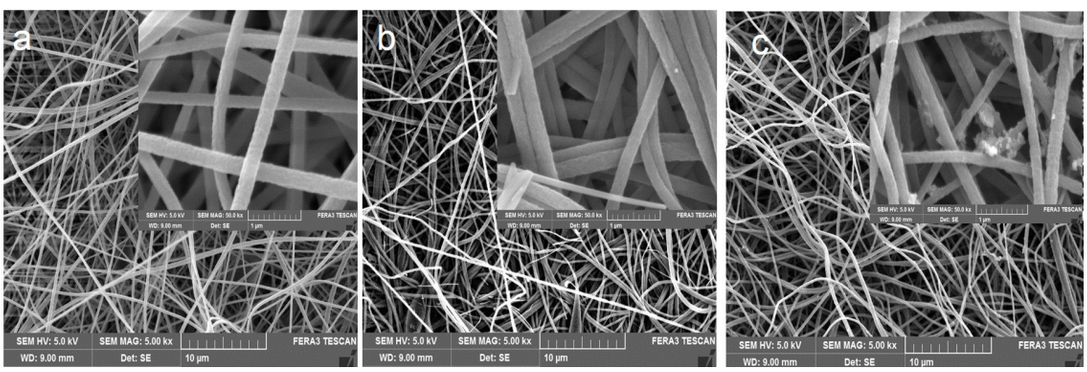

Fig. 8. SEM micrographs of a) electrospun PAN nanofibers, b) HPAN nanofibers, and c) HPAN nanofibers after Pb^{++} ions adsorption.

(L/mmol), Q_m is the maximum metal uptake (mmol/g), while K and n are Freundlich constants indicating adsorption capacity (mmol/g) (L/mmol)^n, and adsorption intensity, respectively.

The experimental adsorption equilibrium data of lead ions fit into these models and the various calculated parameters are listed in Table 5. As shown by the values of R^2 in Table 5, the Langmuir model can be fitted to the adsorption isotherm results of Pb^{++} ions on HPAN nanofiber mats better than the Freundlich model.

According to the Langmuir model, adsorption happens at certain homogeneous sites and, after a sorbate occupies a reaction site, no further adsorption can take place at that site. Thus, lead ions adsorption occurs by forming a monolayer [9].

By using the Langmuir parameters shown in Table 5, the dimensionless separation factor, R_L, can be calculated, which is a criteria of the adsorption tendency between sorbate and adsorbent [8].

$$R_L = \frac{1}{1 + bC_0} \quad (7)$$

The R_L value is classified as $R_L > 1$, $0 < R_L < 1$ and $R_L = 0$, indicating that the adsorption is unfavorable, favorable, and irreversible, respectively [53].

The values of R_L decreased with the increase of the initial concentration of Pb^{++} ions, as shown in Table 6. This indicates that lead ions adsorption was more favorable at higher initial concentrations of Pb^{++} ions [1,8].

3.7. Mechanism of Pb^{++} ions adsorption on HPAN nanofibers

After adsorption process, the fibers were dried to analyze with ATR-FTIR spectroscopy. Fig. 9 shows ATR-FTIR spectra of HPAN nanofibers before and after Pb^{++} ions adsorption. The peak corresponding to each bond could be shifted under influence of neighboring atoms. The peak at 2246 cm^{-1} belongs to the remaining C–N bonds. This peak showed no shift. Therefore, it was concluded that no Pb^{++} ions adsorbed on the C–N bonds. One noticeable shift was observed at 1573 to 1572 cm^{-1} that is attributed to the presence of Pb^{++} ions onto the imine groups. Fig. 10 shows the suggested interaction of Pb^{++} ions and imine groups; The Pb^{++} ions are surrounded with nitrogen atoms under a chelating mechanism.

Table 5
Langmuir and Freundlich constants for Pb^{++} ions adsorption on HPAN nanofiber mats

Model	Parameter		R^2
Langmuir	Q_m = 1.835	b=1.264	0.9559
Freundlich	K_f= 1.115	n=4.945	0.8741

Table 6
R_L for the adsorption of Pb^{++} ions

C_o (mmol/L)	R_L
1.87	0.297
3.22	0.197
5.43	0.127
7.45	0.095
9.87	0.074

3.8. Adsorption kinetics studies

The first and second order rate equations were considered to describe the adsorption kinetics model. Figs. 11a,b give the result of curve fitting based on the following equations for the first order and second order equations, respectively:

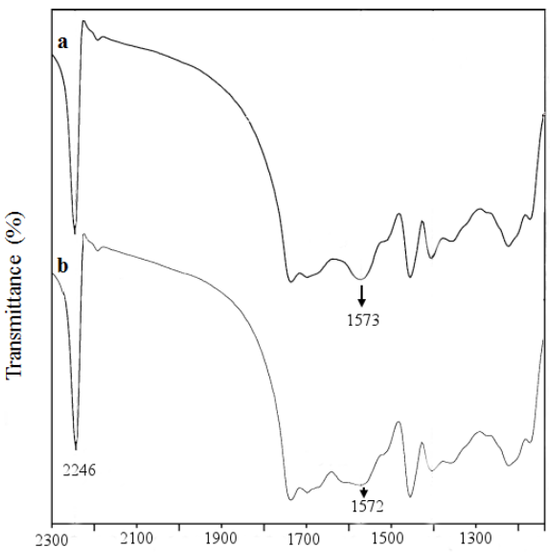

Fig. 9. ATR-FTIR spectra of HPAN nanofibers a) before Pb^{++} ions adsorption b) after Pb^{++} ions adsorption.

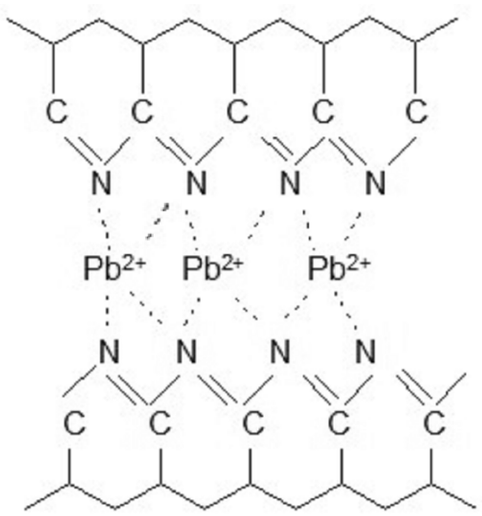

Fig. 10. Proposed mechanism for interaction of Pb^{++} ions and imine groups of modified PAN.

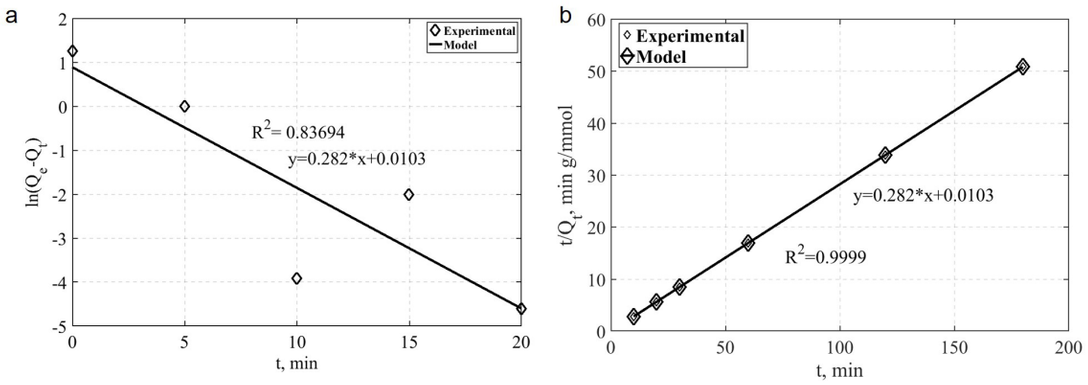

Fig. 11. Adsorption kinetic a) the first order, b) second order rate equations.

$$dq_t/dt = k_1(q_e - q_t) \tag{8}$$

$$dq_t/dt = k_2(q_e - q_t)^2 \tag{9}$$

where q_t and q_e, mmol/g, are the amount of adsorbed Pb^{++} ions at time t and at equilibrium, respectively. k_1 and k_2 are equation rate constants. Integration and rearrangement of the above-mentioned equations could be used in curve fitting:

$$\ln(q_e - q_t) = \ln q_e - k_1 t \tag{10}$$

$$\frac{t}{q_t} = \frac{1}{k_2 q_e^2} + \frac{1}{q_e} t \tag{11}$$

Correlation coefficients, R^2, of both models are given in Figs. 11a, b. It was observed that although the first order kinetic model fitting was not bad, the second order model predicted the adsorption kinetics very well. Therefore, the Pb^{++} ions adsorption onto HPAN nanofibers has a second-order kinetics [32]. The k_2 and q_e values were 13.29 g/mmol·min and 3.54 mmol/g, respectively. Comparison of obtained q_e with the reported value in the literature for microfibers, about 0.2 mmol/g for Pb^{++} ions adsorption on aminated PAN microfibers, shows that adsorption amount and rate in the HPAN nanofibers were very high [5].

4. Conclusion

PAN nanofibers were produced using electrospinning. Nanofibers surface were hydrolyzed to increase metal ion adsorption ability. The simultaneous effects of three variables including hydrolysis reaction temperature, time, and fiber diameter on Pb^{++} ions adsorption were investigated using CCD methodology. By using the numerical optimization, optimum conditions for this adsorption reaction were obtained with the Design Expert 10 software. Both hydrolysis reaction temperature and time increased metal ions adsorption. However, metal ion adsorption decreased by increasing fiber diameter. It is important to mention that the optimized conditions were hydrolysis reaction temperature of 61.6°C, time of 82.1 min, and fiber diameter equal to 280 nm. It was found that Pb^{++} ions adsorption on nanofibers was 20 times that on microfibers under the same conditions. In the system, finding the optimum pH in which adsorption was at the maximum was critically important. In our case, this pH found to be between 4–5. Furthermore, SEM results confirmed formation of nanofibers as well as Pb^{++} ions adsorption. In addition, the as-spun fibers and hydrolyzed fibers showed similar morphology. The Langmuir isotherm fit the adsorption equilibrium data very well, proving a mono-layer adsorption. Moreover, the adsorption kinetics followed the second order kinetic model. Finally, it was demonstrated that using nanofibers increases both the capacity and rate of metal ion adsorption.

References

[1] R. Coşkun, C. Soykan, M. Saçak, Adsorption of copper (II), nickel (II) and cobalt (II) ions from aqueous solution by methacrylic acid/acrylamide monomer mixture grafted poly (ethylene terephthalate) fiber, Sep. Purif. Technol., 49 (2006) 107–114.
[2] P. Karimineghlani, M. Rafizadeh, F. Afshar Taromi, Optimization of Amine Grafting on Polyacrylonitrile Nanofibers Membrane using Central Composite Design, Int. Seminar on Polym. Sci. Technol., 2012, Tehran, Iran.
[3] A.M. Shoushtari, M. Zargaran, M. Abdouss, Preparation and characterization of high efficiency ion-exchange crosslinked acrylic fibers, J. Appl. Poly. Sci., 101 (2006) 2202–2209.
[4] P. Karimineghlani, M. Rafizadeh, F. Afshar Taromi, Adsorption of Copper ions onto Electrospun PAN Nanofiber, Polymer Processing Society 2011, Kish, Iran.
[5] S. Deng, R. Bai, J.P. Chen, Aminated polyacrylonitrile fibers for lead and copper removal, Langmuir, 19 (2003) 5058–5064.
[6] K. Saeed, S. Haider, T.-J. Oh, S.-Y. Park, Preparation of amidoxime-modified polyacrylonitrile (PAN-oxime) nanofibers and their applications to metal ions adsorption, J. Membr. Sci., 322 (2008) 400–405.
[7] S. Deng, R. Bai, J. Chen, Behaviors and mechanisms of copper adsorption on hydrolyzed polyacrylonitrile fibers, J. Colloid Interface Sci., 260 (2003) 265–272.
[8] W. Shen, S. Chen, S. Shi, X. Li, X. Zhang, W. Hu, H. Wang, Adsorption of Cu (II) and Pb (II) onto diethylenetriamine-bacterial cellulose, Carbohydr. Polym., 75 (2009) 110–114.

[9] S. Haider, S.-Y. Park, Preparation of the electrospun chitosan nanofibers and their applications to the adsorption of Cu (II) and Pb (II) ions from an aqueous solution, J. Membr. Sci., 328 (2009) 90–96.
[10] C. Shen, Y. Chang, L. Fang, M. Min, C. Xiong, Selective removal of copper with polystyrene-1, 3-diaminourea chelating resin: synthesis and adsorption studies, New J. Chem., 40 (2016) 3588–3596.
[11] C. Xiong, Q. Jia, X. Chen, G. Wang, C. Yao, Optimization of polyacrylonitrile-2-aminothiazole resin synthesis, characterization, and its adsorption performance and mechanism for removal of Hg (II) from aqueous solutions, Ind. Eng. Chem. Res., 52 (2013) 4978–4986.
[12] A. Formhals (1934). Process and apparatus for preparing artificial threads. US Patent, 1975504.
[13] D. Fallahi, M. Rafizadeh, N. Mohammadi, B. Vahidi, Effects of feed rate and solution conductivity on jet current and fiber diameter in electrospinning of polyacrylonitrile solutions, e-Polymers, 9 (2009) 1250–1257.
[14] P. Karimineghlani, M. Rafizadeh, F. Afshar Taromi. Grafting of Amine Groups to Polyacrylonitrile Nanofibers for Metal Ion Adsorption, Int. Seminar on Polym. Sci. Technol., 2009, Tehran, Iran.
[15] T. Subbiah, G. Bhat, R. Tock, S. Parameswaran, S. Ramkumar, Electrospinning of nanofibers, J. Appl. Polym. Sci., 96 (2005) 557–569.
[16] E.M. Sullivan, P. Karimineghlani, F. Gencarella, R. Puvvada, B. Wang, R. Gerhardt, M. Naraghi, K. Kalaitzidou, Processing And Characterization Of Carbon Nanotube/Polylactic Acid Nanocomposite Films. 20th Int. Conference on Composite Materials. 2015, Copenhagen, Denmark.
[17] E.M. Sullivan, P. Karimineghlani, M. Naraghi, R.A. Gerhardt, K. Kalaitzidou, The effect of nanofiller geometry and compounding method on polylactic acid nanocomposite films, Eur. Polym. J., 77 (2016) 31–42.
[18] C. Shao, H.-Y. Kim, J. Gong, B. Ding, D.-R. Lee, S.-J. Park, Fiber mats of poly (vinyl alcohol)/silica composite via electrospinning, Mater. Lett., 57 (2003) 1579–1584.
[19] M. Irani, A.R. Keshtkar, M.A. Moosavian, Removal of cadmium from aqueous solution using mesoporous PVA/TEOS/APTES composite nanofiber prepared by sol–gel/electrospinning, Chem. Eng. J., 200 (2012) 192–201.
[20] Q.P. Pham, U. Sharma, A.G. Mikos, Electrospinning of polymeric nanofibers for tissue engineering applications: a review, Tissue Eng., 12 (2006) 1197–1211.
[21] Y. You, B.M. Min, S.J. Lee, T.S. Lee, W.H. Park, In vitro degradation behavior of electrospun polyglycolide, polylactide, and poly (lactide-co-glycolide), J. Appl. Polym. Sci., 95 (2005) 193–200.
[22] H. Liu, J. Kameoka, D.A. Czaplewski, H. Craighead, Polymeric nanowire chemical sensor, Nano Lett., 4 (2004) 671–675.
[23] C. Bamford, K. Al-Lamee, M. Purbrick, T. Wear, Studies of a novel membrane for affinity separations: I. Functionalisation and protein coupling, J. Chromatogr. A., 606 (1992) 19–31.
[24] Z. Ma, K. Masaya, S. Ramakrishna, Immobilization of Cibacron blue F3GA on electrospun polysulphone ultra-fine fiber surfaces towards developing an affinity membrane for albumin adsorption, J. Membr. Sci., 282 (2006) 237–244.
[25] Z. Ma, M. Kotaki, S. Ramakrishna, Electrospun cellulose nanofiber as affinity membrane, J. Membr. Sci., 265 (2005) 115–123.
[26] P. Kampalanonwat, P. Supaphol, Preparation and adsorption behavior of aminated electrospun polyacrylonitrile nanofiber mats for heavy metal ion removal, ACS Appl. Mater. Interfaces., 2 (2010) 3619–3627.
[27] P. Kampalanonwat, P. Supaphol, Preparation of hydrolyzed electrospun polyacrylonitrile fiber mats as chelating substrates: a case study on copper (II) ions, Ind. Eng. Chem. Res., 50 (2011) 11912–11921.
[28] R. Zhao, X. Li, B. Sun, Y. Li, Y. Li, R. Yang, C. Wang, Branched polyethylenimine grafted electrospun polyacrylonitrile fiber membrane: a novel and effective adsorbent for Cr (vi) remediation in wastewater, J. Mater. Chem. A., 5 (2017) 1133–1144.
[29] R. Zhao, X. Li, B. Sun, H. Ji, C. Wang, Diethylenetriamine-assisted synthesis of amino-rich hydrothermal carbon-coated electrospun polyacrylonitrile fiber adsorbents for the removal of Cr (VI) and 2, 4-dichlorophenoxyacetic acid, J. Colloid Interface Sci., 487 (2017) 297–309.
[30] C.A. Bode-Aluko, O. Pereao, G. Ndayambaje, L. Petrik, Adsorption of toxic metals on modified Polyacrylonitrile nanofibres: A review, Water Air Soil Pollut., 228 (2017) 35.
[31] F. Liu, X. Wang, B.-Y. Chen, S. Zhou, C.-T. Chang, Removal of Cr (VI) using polyacrylonitrile/ferrous chloride composite nanofibers, J. Taiwan Inst. Chem. Eng., 70 (2017) 401–410.
[32] P.K. Neghlani, M. Rafizadeh, F.A. Taromi, Preparation of aminated-polyacrylonitrile nanofiber membranes for the adsorption of metal ions: Comparison with microfibers, J. Hazard. Mater., 186 (2011) 182–189.
[33] F. Oughlis-Hammache, N. Hamaidi-Maouche, F. Aissani-Benissad, S. Bourouina-Bacha, Central composite design for the modeling of the phenol adsorption process in a fixed-bed reactor, J. Chem. Eng. Data., 55 (2010) 2489–2494.
[34] P. Sharma, L. Singh, N. Dilbaghi, Response surface methodological approach for the decolorization of simulated dye effluent using Aspergillus fumigatus fresenius, J. Hazard. Mater., 161 (2009) 1081–1086.
[35] R.H. Myers, D.C. Montgomery, G.G. Vining, C.M. Borror, S.M. Kowalski, Response surface methodology: a retrospective and literature survey, J. Quality Technol., 36 (2004) 53.
[36] B. Preetha, T. Viruthagiri, Application of response surface methodology for the biosorption of copper using Rhizopus arrhizus, J. Hazard. Mater., 143 (2007) 506–510.
[37] R. Liu, Y. Li, H. Tang, Synthesis and characteristics of chelating fibers containing imidazoline group or thioamide group, J. Appl. Polym. Sci., 83 (2002) 1608–1616.
[38] A. Khataee, Application of central composite design for the optimization of photo-destruction of a textile dye using UV/S2O82-process, Pol. J. Chem. Technol., 11 (2009) 38–45.
[39] M. Nowak, A. Seubert, Application of experimental design for the characterisation of a novel elution system for high-capacity anion chromatography with suppressed conductivity detection, J. Chromatogr. A., 855 (1999) 91–109.
[40] P. Karimineghlani, E. Emmons, M.J. Green, P. Shamberger, S.A. Sukhishvili, A temperature-responsive poly(vinyl alcohol) gel for controlling fluidity of an inorganic phase change material, J. Mater. Chem. A., (2017). DOI: 10.1039/C7TA02897K.
[41] G.G. Vining, S. Kowalski, (2010). Statistical methods for engineers.
[42] M. Ahmadi, F. Vahabzadeh, B. Bonakdarpour, M. Mehranian, Empirical modeling of olive oil mill wastewater treatment using loofa-immobilized Phanerochaete chrysosporium, Process Biochem., 41 (2006) 1148–1154.
[43] Z. Salehi, F. Vahabzadeh, M. Sohrabi, S. Fatemi, H.T. Znad, Statistical medium optimization and biodegradative capacity of Ralstonia eutropha toward p-nitrophenol, Biodegradation, 21 (2010) 645–657.
[44] R.F. Gunst, Response surface Methodology: Process and product Optimization Using Designed Experiments. 1996, Taylor & Francis, Technometrics, Volume 38, Issue 3.
[45] M. McComb, H. Gesser, Preparation of polyacryloamidoxime chelating cloth for the extraction of heavy metals from water, J. Appl. Polym. Sci., 65 (1997) 1175–1192.
[46] J.-A. Park, J.-K. Kang, S.-C. Lee, S.-B. Kim, Electrospun poly (acrylic acid)/poly (vinyl alcohol) nanofibrous adsorbents for Cu (ii) removal from industrial plating wastewater, RSC Adv., 7 (2017) 18075–18084.
[47] J. Xiong, C. Jiao, C. Li, D. Zhang, H. Lin, Y. Chen, A versatile amphiprotic cotton fiber for the removal of dyes and metal ions, Cellulose, 21 (2014) 3073–3087.
[48] Y. Xu, J. Sun, H. Chen, L. Bai, Cobalt (III) acetylacetonate initiated RAFT polymerization of acrylonitrile and its application in removal of methyl orange after electrospinning, RSC Adv., 5 (2015) 58393–58402.
[49] F.L. Williams, K. Baron, Lead, sulfur and phosphorus interactions with platinum and palladium metal foils, J. Catal., 40 (1975) 108–116.

[50] G. Carturan, G. Deganello, T. Boschi, U. Belluco, A palladium–lead bonded complex, J. Chem. Soc. A: Inorganic, Physical, Theoretical, (1969) 1142–1144.
[51] B. Crociani, M. Nicolini, D. Clemente, G. Bandoli, Some palladium (II) and platinum (II) lead bonded complexes, J. Organomet. Chem., 49 (1973) 249–256.
[52] M.E. Argun, S. Dursun, M. Karatas, M. Gürü, Activation of pine cone using Fenton oxidation for Cd (II) and Pb (II) removal, Bioresour. Technol., 99 (2008) 8691–8698.
[53] Y.-T. Zhou, H.-L. Nie, C. Branford-White, Z.-Y. He, L.-M. Zhu, Removal of Cu^{2+} from aqueous solution by chitosan-coated magnetic nanoparticles modified with α-ketoglutaric acid, J. Colloid Interface Sci., 330 (2009) 29–37.